dhanes@usgs.gov
01/26/2005 12:59 PM

To: men_lib@usgs.gov
cc:
Subject: USGS Library - INTERNAL Reference Request

USGS Library Electronic Reference Service - INTERNAL Reference Request

Name: Dan Hanes
Address:
, CA

Email: dhanes@usgs.gov ← scan to

Question: Reconstruction of ancient sea conditions with an example from the Swiss Molasse
Marine Geology, Volume 60, Issues 1-4, August 1984, Pages 455-473
Philip A. Allen

530
M337
v.60
no.1-4

U.S. GEOLOGICAL SURVEY LIBRARY
WESTERN REGION
345 MIDDLEFIELD ROAD, MS-955
MENLO PARK, CALIFORNIA 94025-3591
REFERENCE: (650) 329-5027
CIRCULATION: (650) 329-5026
FAX: (650) 329-5132
(650) 329-5097
email: men_lib@usgs.gov

From: Lorrie Gallagher
lgallagher@usgs.gov
(650) 329-5008

This is an article you have requested. If you have a question or a problem with this document, please contact me.

7/1/2002
h:scansheet.doc

MARINE GEOLOGY

VOL. 59 (1984)

Marine Geology, 60 (1984) 455—473
Elsevier Science Publishers B.V., Amsterdam — Printed in The Netherlands

RECONSTRUCTION OF ANCIENT SEA CONDITIONS WITH AN EXAMPLE FROM THE SWISS MOLASSE

PHILIP A. ALLEN

Department of Geology, University College, P.O. Box 78, Cardiff CF1 1XL (United Kingdom)

(Received March 15, 1983; revised and accepted August 29, 1983)

ABSTRACT

Allen, P.A., 1984. Reconstruction of ancient sea conditions with an example from the Swiss Molasse. In: B. Greenwood and R.A. Davis, Jr. (Editors), Hydrodynamics and Sedimentation in Wave-Dominated Coastal Environments. Mar. Geol., 60: 455—473.

Ancient sea conditions can be estimated from the grain size, spacing and steepness of preserved ripple-marks. The element of greatest uncertainty in such reconstructions is the relationship between near-bed orbital diameter of water particles and the ripple spacing. This relationship is simple for vortex ripples of high steepness but is problematical for the low-steepness forms known as post-vortex, rolling-grain or anorbital ripples.

The existence field for wave ripples is between the threshold velocity for sediment movement and the onset of sheet flow, most low-steepness forms occurring close to the bed planation threshold. A range of maximum period of formative waves can be obtained using combinations of orbital diameter and orbital velocity, assuming linear wave theory to be a reasonable approximation.

Probable wave heights, wave lengths and water depths can be investigated using the transformation of wave parameters in shallowing waters and the constraints on wave dimensions provided by the wave-breaking condition. Given reasonable estimates of wave height, crude estimates of wave power allow a comparison of ancient wave-influenced sequences with modern counterparts.

Wave ripple-marks preserved in the Upper Marine Molasse of western Switzerland have been investigated. Results, which are in agreement with regional geology, suggest deposition in a seaway of approximately 100 km width, where moderate period waves (T = 3—6 s) were generated. The depositional facies belts were adjusted to the prevailing waves, tides and fluvial outflows.

INTRODUCTION

Since Harms (1969), Tanner (1971) and Komar (1974), with varying degrees of rigour, proposed the use of preserved wave ripple-marks in reconstructing ancient wave conditions, surprisingly few ancient sequences have been analysed in this way. Further encouragements both from theoretical and empirical (Clifton, 1976; Allen, 1979; Dingler, 1979; Miller and Komar, 1980a) and field studies (Newton, 1968; Cook and Gorsline, 1972; Stone and Summers, 1972; Dingler and Inman, 1977; Miller and Komar, 1980b) have not yet resulted in a flourish of case-studies of ancient marine

0025-3227/84/$03.00

or lacustrine sedimentary basins. Allen (1981a) analysed a Devonian lacustrine basin-fill and Homewood and Allen (1981) studied the marine sediments of the "Upper Marine Molasse" of Switzerland, but to the author's knowledge very few oceanic coastline deposits have been comprehensively treated.

There are, of course, formidable assumptions and approximations which must be made in quantifying ancient wave conditions (Allen, 1981b), but with knowledge of the pitfalls, important insights into palaeoenvironments and processes can be acquired. Without knowledge of the assumptions and approximations, spurious results will be obtained. The purpose of this paper is to describe the methods used by Homewood and Allen (1981) in their analysis of the Upper Marine Molasse of western Switzerland and to synthesize some of the more important elements of particular uncertainty in the reconstruction of ancient sea conditions. This contribution therefore acts as something of a cookbook which may encourage workers to analyse or re-analyse quantitatively their ancient wave-influenced sequences.

METHODS

Are they wave ripple-marks?

Boersma (1970) distinguished a number of features thought to be characteristic of wave-generated ripple cross-lamination, including irregular or catenary-arcuate lower bounding surfaces, bundled upbuilding of cross-sets within ripple cross-laminated lenses, chevron structures, cross-stratal offshoots and form-discordancy. Tanner (1967) and Reineck et al. (1971) likewise summarized wave ripple-marks in terms of ripple steepness, symmetry and crestal arrangement in plan. Wave ripple-marks characteristically have straight crestlines which commonly bifurcate, low ripple indices and symmetrical to near-symmetrical profiles.

There have been relatively few studies of the natural variability in morphology and structure of wave ripple-marks. A very wide spectrum of ripple morphologies has been described from experimental studies (Bagnold, 1946; Manohar, 1955; Dingler, 1974; Sleath, 1976), ranging from the very flat varieties which have variously been termed "rolling grain ripples" (Bagnold, 1946; Sleath, 1976; Allen, 1979) and "post-vortex ripples" (Dingler, 1974; Dingler and Inman, 1976) to the very steep varieties termed 'vortex ripples' (Bagnold, 1946; Sleath, 1976) or 'orbital ripples' (Clifton, 1976). The identification of these ripple types in natural environments has not always been unequivocal.

The relationship between orbital diameter of water particles and ripple spacing

Miller and Komar (1980a) summarized laboratory experiments seeking to determine the relationship between near-bed orbital diameter and ripple

spacing. Oscilla
Sleath, 1975,
1969; Chan e
Lofquist, 1977
and Watanabe,
and Inman, 19
data, for small
diameter (d_0) a

$\lambda = 0.65\, d_0$

(Miller and Ko
best fit to this
demonstrated i
Hom-Ma et al.,
orbital diamete
function of grai

$\lambda_{max} = 0.0028$

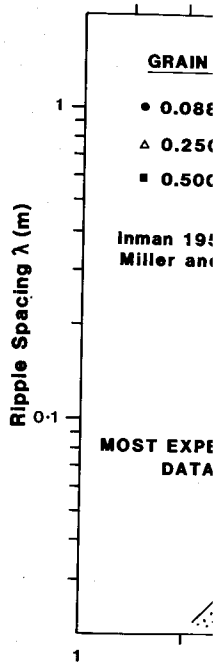

Fig.1. Relationship
spacing (λ) with da
d_0 and $\lambda \gtrsim 0.2$ m.
height. Modified fro

spacing. Oscillating beds (Bagnold, 1946; Manohar, 1955; Kalkanis, 1964; Sleath, 1975, 1976), oscillating water tunnels or U-tubes (Carstens et al., 1969; Chan et al., 1972; Mogridge, 1973; Brebner and Reidel, 1973; Lofquist, 1977, 1978) and wave flumes (Yalin and Russell, 1962; Horikawa and Watanabe, 1967; Mogridge and Kamphuis, 1973; Dingler, 1974; Dingler and Inman, 1977) have been used to study oscillatory flows. From these data, for small orbital diameters, the relationship between near-bed orbital diameter (d_0) and ripple spacing (λ) is very simple (Fig.1):

$$\lambda = 0.65\, d_0 \qquad (1)$$

(Miller and Komar, 1980, p.178), the flume and U-tube data providing the best fit to this curve. Equation 1 has a weak Reynolds number dependence demonstrated independently by Sleath (1976) and Japanese workers (e.g. Hom-Ma et al., 1965), but can be neglected here for simplicity. As near-bed orbital diameter increases eq.1 no longer holds, becoming invalid as a function of grain size:

$$\lambda_{max} = 0.0028\, D^{1.68} \qquad (2)$$

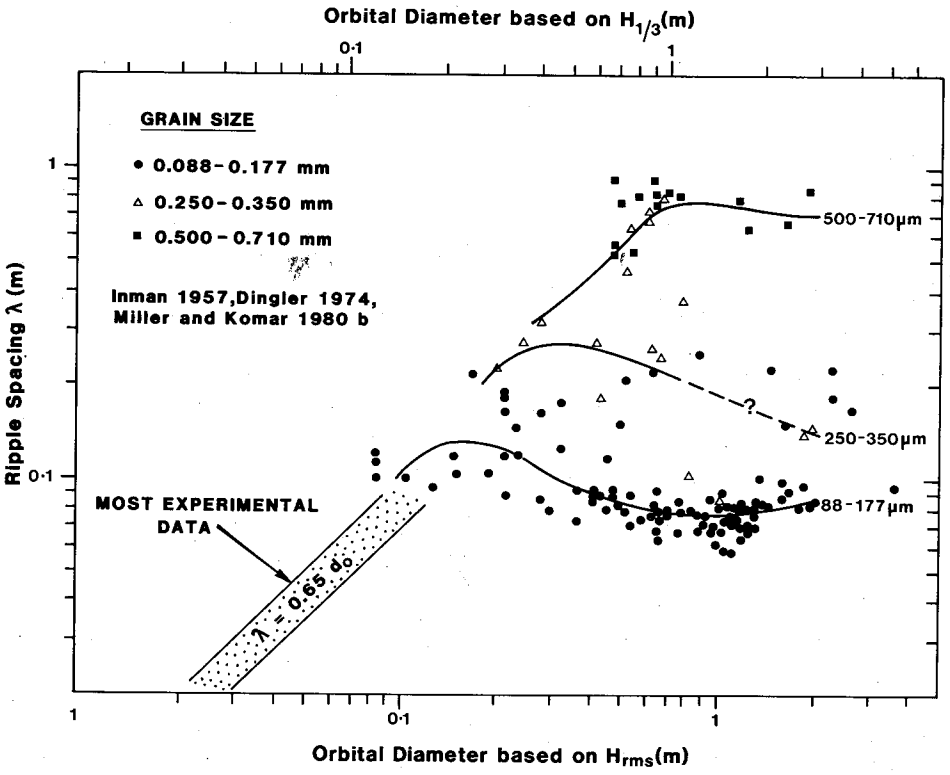

Fig.1. Relationship between near-bed orbital diameter of water particles (d_0) and ripple spacing (λ) with data sources indicated. Note the poor correlation between d_0 and λ for d_0 and $\lambda \gtrsim 0.2$ m. $H_{1/3}$ is significant wave height, H_{rms} is root mean square of wave height. Modified from Miller and Komar (1980b).

(Miller and Komar, 1980, p.180) where D is the median grain-diameter in microns and λ_{max} is in centimetres.

Allen (1979) showed that ripple steepness is an important factor influencing wave reconstructions. He plotted the data of Inman (1957), Kennedy and Falcon (1965), Manohar (1955), Inman and Bowen (1963), Hom-Ma et al. (1965), Carstens et al. (1969), Lofquist (1978) and Sleath and Ellis (1978) on a dimensionless ripple spacing (λ/D) versus dimensionless orbital diameter (d_0/D) diagram with ripple steepness as a further variable (Fig.2). A range of dimensionless orbital diameters could be obtained for a given ripple steepness. Equation 1 then merely represented one limit on Allen's fig.2 (1979, p.676) for vortex ripples, the other limit being determined for post-vortex or rolling grain ripples (Sleath, 1975, 1976) as:

$$0.036 < \lambda/d_0 < 0.059 \qquad (3)$$

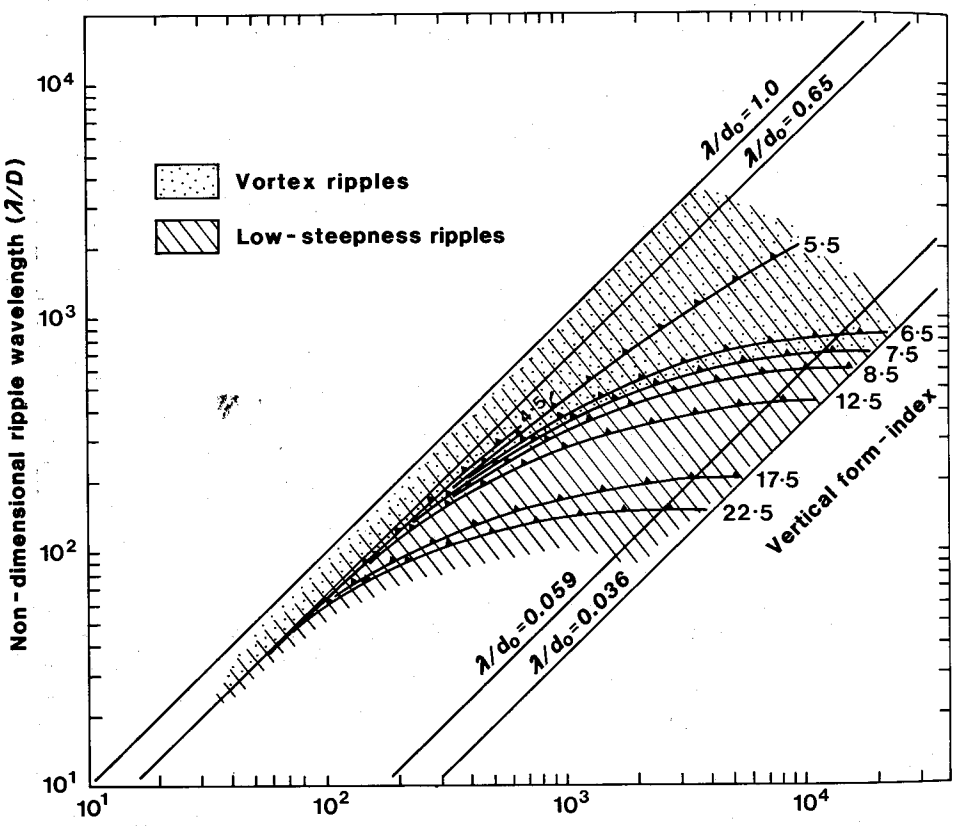

Fig.2. Occurrence of wave ripple-marks as a function of dimensionless ripple spacing (λ/D) and dimensionless near-bed orbital diameter of water particles (d_0/D). The lower limit of ripple occurrence is given by λ/d_0 = 0.65 or 1.0 and the upper limits for given ripple steepnesses (vertical form indices) are given by the series of curves. Note that the curves represent the upper limit of d_0/D and are not isopleths. After Allen (1979, p.676).

Allen (1981) suggeste
inevitably led to an u
making wave reconstru

The relationship be
can be expressed as:

$\lambda = F(d_0, \nu, D, \rho_s, \rho, g,$

Since $U_0 = \omega d_0/2$, Sl
tween orbital diameter
tion of four dimension

$$\frac{d_0}{2\lambda} = F[\beta D, R, \rho_s/\rho, (\rho_s$$

where $R = U_0/(\omega\nu)^{1/2}$
It can be seen that th
contains U_0. Only prio
equations (1976, p. 78

Clearly, the best re
unambiguous relations
Such vortex ripple-ma
over a steep crest. B
and Allen (1979) sugge
form index, VFI; Buch
and Inman (1977) sta
worth emphasising tha
ment and flow-related
dominant control on t
be exercised in analysi
and it is recommend
possessing vertical form

The critical velocities f

The critical thresho
Shields parameter, and
viscosity (μ), grain di
particles (d_0). For grai
relation is:

$\rho U_t^2/(\rho_s - \rho)gD = 0.21$

which is based exclus
laminar boundary laye
Miller (1973) suggested

$\rho U_t^2/(\rho_s - \rho)gD = 0.46$

derived from the dat
turbulent boundary lay

Allen (1981) suggested that the use of a wide range of ripple steepness inevitably led to an unacceptably wide range of estimated orbital diameters, making wave reconstructions hazardous.

The relationship between ripple spacing and grain and flow parameters can be expressed as:

$$\lambda = F(d_0, \nu, D, \rho_s, \rho, g, \omega) \tag{4}$$

Since $U_0 = \omega d_0/2$, Sleath (1976) was able to express the relationship between orbital diameter and ripple spacing for "rolling grain ripples" as a function of four dimensionless variables:

$$\frac{d_0}{2\lambda} = F[\beta D, R, \rho_s/\rho, (\rho_s - \rho)gD/\rho\omega\nu] \tag{5}$$

where $R = U_0/(\omega\nu)^{1/2}$ is a form of wave Reynolds number and $\beta = (\omega/2\nu)^{1/2}$. It can be seen that three of these dimensionless groups contain ω and one contains U_0. Only prior knowledge of U_0 and an iterative solution of Sleath's equations (1976, p. 78) would allow a solution to be made.

Clearly, the best results will come from those ripple-marks for which an unambiguous relationship between orbital diameter and ripple spacing exists. Such vortex ripple-marks are defined by the incidence of flow separation over a steep crest. Bagnold (1946), J.F.A. Sleath (pers. commun., 1979) and Allen (1979) suggested limiting ripple steepnesses (expressed as a vertical form index, VFI; Bucher 1919) of 8.0, 8.3 and 7.5, respectively, and Dingler and Inman (1977) stated an average value of 6.7 for vortex ripples. It is worth emphasising that ripple steepness is a function of several fluid, sediment and flow-related variables but that ripple steepness alone is the predominant control on the existence of vortex ripples. Extreme caution must be exercised in analysing low-steepness ripple-marks for wave reconstructions and it is recommended that attention is focused on vortex ripple-marks possessing vertical form indices of less than 7.5 and certainly less than 10.

The critical velocities for wave ripple formation

The critical threshold for entrainment under waves is given by a modified Shields parameter, and is determined by grain and fluid density (ρ_s, ρ), fluid viscosity (μ), grain diameter (D) and near-bed orbital diameter of water particles (d_0). For grain sizes of less than 0.5 mm, Komar and Miller's (1973) relation is:

$$\rho U_t^2/(\rho_s - \rho)gD = 0.21\ (d_0/D)^{1/2} \tag{6}$$

which is based exclusively on Bagnold's (1946) data and corresponds to laminar boundary layers. For grain sizes greater than 0.5 mm, Komar and Miller (1973) suggested the expression:

$$\rho U_t^2/(\rho_s - \rho)gD = 0.46\,\pi\ (d_0/D)^{1/4} \tag{7}$$

derived from the data of Rance and Warren (1969) which applies to turbulent boundary layers.

Ripple steepness is intimately related to processes in the wave boundary layer. It is the near-bed curvature-related drift velocities (Sleath, 1975, 1976) which are directly responsible for wave ripple-mark formation (Bagnold, 1946; Kaneko and Honji, 1979), whereas it is the purely oscillatory (simple harmonic) component which causes most grain movement. Allen (1979, fig.1, p. 675) plotted the purely oscillatory component, U_{max}, against grain diameter for a range of steepness values (Fig.3). Together with the analysis of Komar and Miller (1976), Allen's compilation shows that wave ripple-marks occur at orbital velocities well above those at the threshold condition, up to the point at which ripples are destroyed and sheet flow commences (Fig.3).

Komar and Miller (1976) gave the critical relative stress for ripple disappearance as a function of grain size alone, as:

$$\theta_c = 0.413\, D^{-0.396} \qquad (8)$$

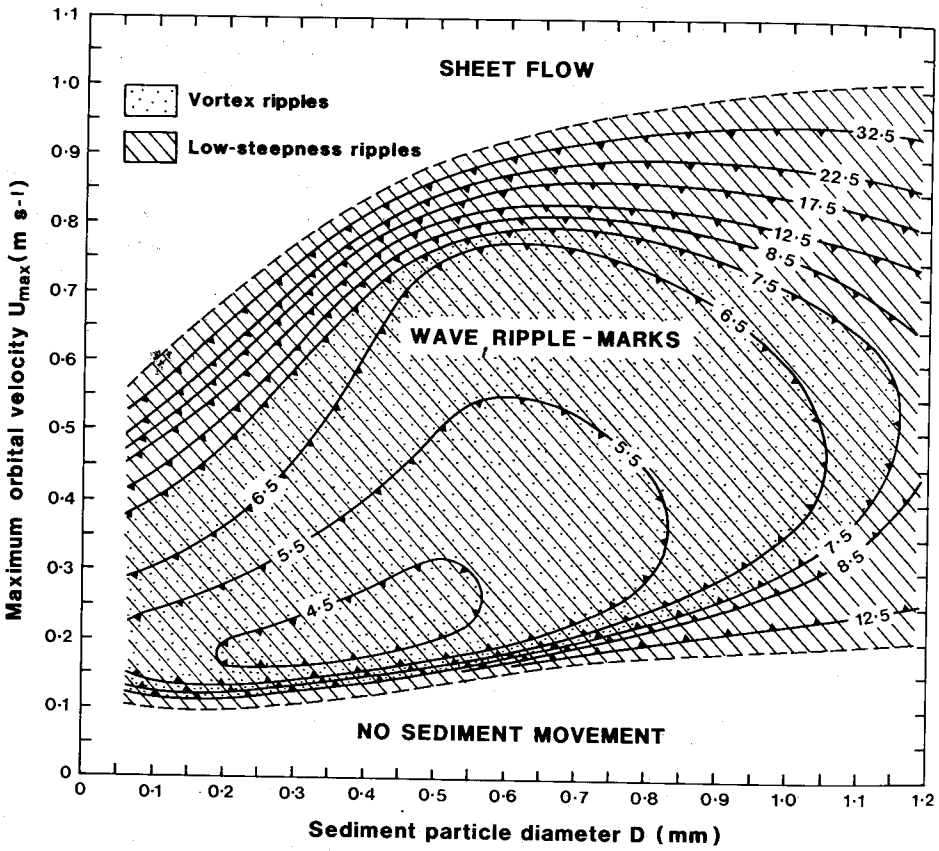

Fig.3. Occurrence of wave ripple-marks as a function of maximum near-bed orbital velocity of water particles (U_{max}) and grain size of sediment (D_{50}). The curves for ripple steepness (vertical form index) enclose the existence-field of ripple-marks with a given steepness. After Allen (1979, p.675).

or in terms of g

$\theta_c = 4.40\,(U_{max}$

both based on

directly to Aller

Calculation of u

Using linear

Méhauté et al.,

and velocities to

$U_{max} = \pi d_0/T$

Equation 10 ind

threshold veloci

threshold condit

Maximum wave

conditions. If o

above, a range

obtained.

The rationale

determined by v

on wind speed

typical storm co

derive fetch limi

refined by Bretsc

limited seas the

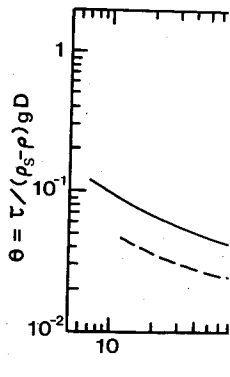

Fig. 4. Occurrence o

relative stress (θ) and

on the laboratory da

et al. (1969) and the

structed from the da

Bagnold (1956, 1966

or in terms of grain Reynolds number as:

$$\theta_c = 4.40\,(U_{max} D/\nu)^{-0.333} \quad (9)$$

both based on Manohar's (1955) data (Fig.4). The simpler method is to go directly to Allen's (1979) fig.1 which is based on a far wider range of data.

Calculation of wave period

Using linear wave theory, which is adequate for these purposes (Le Méhauté et al., 1969), it is possible to relate near-bottom orbital diameters and velocities to wave period (T) with the simple expression:

$$U_{max} = \pi d_0/T \quad (10)$$

Equation 10 indicates that although the entire range of conditions from the threshold velocity to the destruction velocity should be studied, it is the threshold condition (minimum U_0) which gives the maximum wave period. Maximum wave periods are of greater interest in reconstructing ancient sea conditions. If one experiments with the limits of the range of d_0 obtained above, a range of T for both the threshold and destruction condition is obtained.

The rationale behind calculating T is that the period of gravity waves is determined by wind strength, duration and fetch. Placing reasonable limits on wind speed and duration (for example, for typical fair-weather and typical storm conditions), it is possible to use wave forecasting methods to derive fetch limits for calculated wave periods (Sverdrup and Munk, 1946; refined by Bretschneider, 1970, or Darbyshire and Draper, 1963). In fetch-limited seas the analysis of Neumann (1953) is particularly useful (Fig.5).

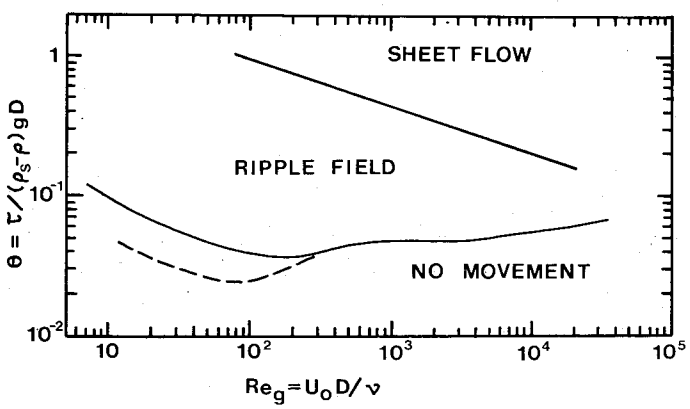

Fig. 4. Occurrence of wave ripple-marks as a function of a Bagnold (1963)-Shields (1936) relative stress (θ) and grain Reynolds number (Re_g). The ripple existence-field was based on the laboratory data of Manohar (1955), Horikawa and Watanabe (1967) and Carstens et al. (1969) and the field data of Inman (1957). The bed planation threshold was constructed from the data of Manohar (1955) and supported by the theoretical criterion of Bagnold (1956, 1966). After Komar and Miller (1975, p.701).

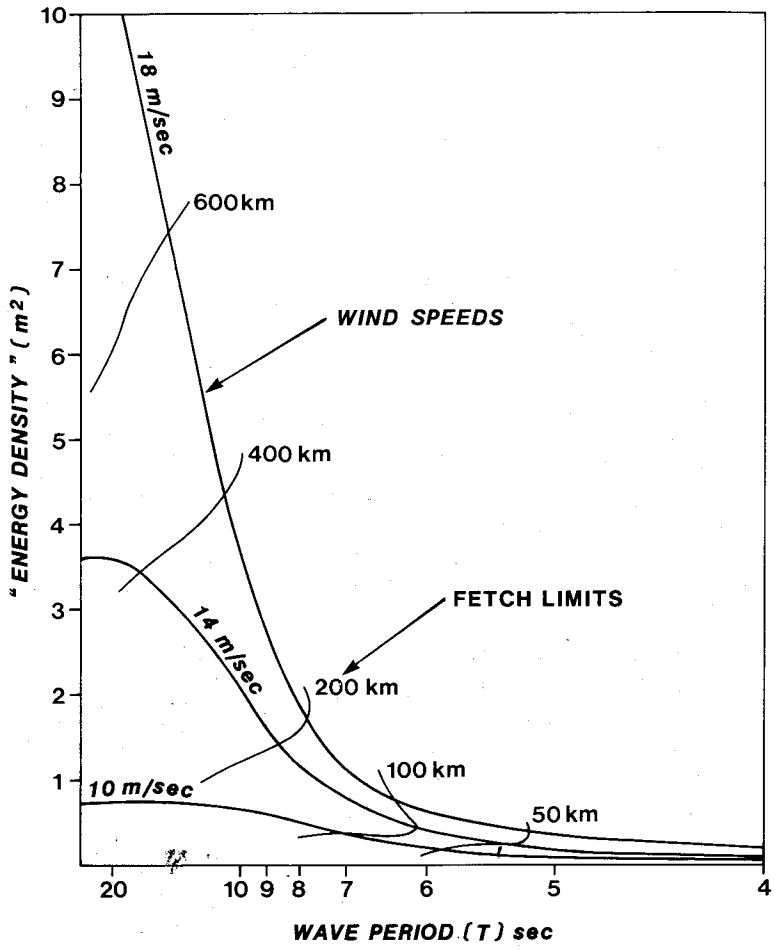

Fig.5. The energy density spectra for sea conditions where fetch is limiting, after Neumann (1953).

Calculated fetches for ancient waves are an important asset in palaeogeographical studies. Homewood and Allen (1981) used fetch length calculated from Miocene wave ripple-marks to confirm traditional views, based on the distribution of marine facies, on the size of the peri-Alpine sea in Switzerland. Allen (1981) used fetch data to postulate the extent of a Devonian lacustrine basin where outcrops were incomplete.

Simulation of wavelength, wave height and water depth

The orbital diameter of water particles near the bed is the result of a wave of period T, height H and wavelength L acting in water depth h. It follows that it is impossible to obtain a unique solution to H, L and h; it is only possible to obtain combinations of parameters. This is why estimation of H, L and h is well suited to computer simulation (see Komar, 1974, for instance).

Because deep-water waves are unaffected by water depth, it is possible to construct deep-water wavelength based purely on wave period, as follows:

$$L_\infty = gT^2/2\pi \tag{11}$$

which is a simplification of the general case:

$$L = (gT^2/2\pi) \tanh\left(\frac{2\pi h}{L}\right) \tag{12}$$

As the wave travels into shallower water its form changes so that orbital diameter of water particles near the bottom is given by:

$$d_0 = H/\sinh(2\pi h/L) \tag{13}$$

It is necessary therefore to study the transformations which take place in a wave of known period T as it moves into shallower water. This can be done in various ways, but a relatively painless method is to calculate h/L_∞ for the primary field of interest for water depth and use the graphs for Airy wave transformations provided by Wiegel (1964) (Fig.6). Alternatively Eckart (1952) gave the approximation:

$$L = L_\infty \text{ abs}[\tanh(2\pi h/L_\infty)] \tag{14}$$

The variation of H is of particular interest since it affects near-bed orbital diameter. Assuming that in order to form the observed ripple-marks the waves possessed finite near-bottom orbital diameters (i.e., the formative waves were not deep-water waves), eq.13 can be used to obtain wave height.

Wave breaking

There is another limit which is critical to the validity of the reconstructed wave parameters, that of wave breaking. Miche (1944) gives the limiting steepness for waves in water of finite depth as:

$$(H/L)_{\text{lim}} = 0.142 \tanh(2\pi h/L) \tag{15}$$

and in progressively shallower water (McCowan, 1894) waves break at:

$$(H/h)_{\text{lim}} = 0.78 \tag{16}$$

Equation 16 is sensitive to beach slope (Ippen and Kulin, 1955). For small slopes ($\tan\beta < 0.07$):

$$0.72 < (H/h)_{\text{lim}} < 1.18 \tag{17}$$

and for a reasonable beach slope of 0.003:

$$(H/h)_{\text{lim}} = 0.88 \tag{18}$$

which is in close agreement with eq.16. Only rarely do geologists have data on ancient beach slope, so it is normal to simply implement eqs. 15 and 16.

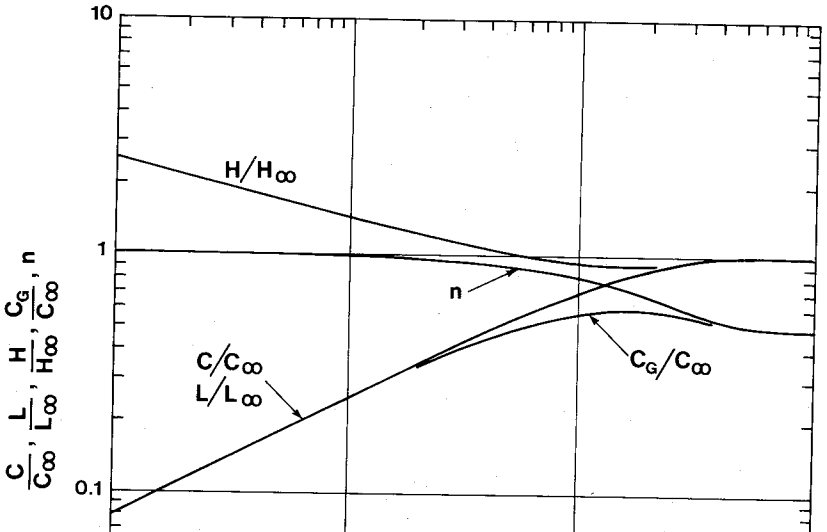

Fig.6. The shoaling transformations for Airy waves as functions of the ratio of water depth to deep-water wavelength, h/L_∞. C, C_g and C_∞ are wave celerity (phase velocity), group velocity and deep-water celerity. H and H_∞ are wave height and deep-water wave height. L and L_∞ are surface wavelength and deep-water wavelength. n is a shoaling coefficient relating wave celerity to group velocity. After Wiegel (1964).

Energy flux (wave power)

The motion of waves produces a transfer of energy over the sea surface which is of great interest to physical oceanographers and coastal engineers. A wave train possesses a total energy made up of two components. The potential energy component is caused by water particles being displaced from the still water level, and the kinetic energy component accounts for the orbital motions of water particles. The total energy is given by:

$$E = \rho g H^2/8 \qquad (19)$$

(Teleki, 1972, p.38; Madsen, 1976, p.72) where E is a surface energy density per unit width of wave crest. The rate at which this energy is propagated in the direction of wave advance is the energy flux (or wave power), and is directly related to the velocity of the wave train (group velocity C_g) rather than the phase velocity of individual waveforms. The energy flux per unit length of wave crest is:

$P = \rho g H^2 C_g/8$

Group velocity can be
tions as the dimensionl
wave phase velocity (ce

$C = L/T = (gT/2\pi)\tanh($

where $C = C_\infty = gT/2\pi$ i

Energy flux for rec
lowing waters, the rati
flux providing an index
used estimates of energ
Sea of Switzerland by c
Coleman and Wright (19

THE UPPER MARINE MOI

The wedge of Tertiar
tionally subdivided into
lowermost, of Oligocer
represents offshore mu
wave-dominated shoreli
water Molasse compris
some playa and lacustr
Molasse of Miocene (Bur
shallow marine sandstor
uppermost unit, the Up
and fluviatile clastics and

The Upper Marine Mo
of the Alps (Fig.7B) wh
and southwestward int
throughout the Upper M
in the vicinity of Fribo
spectacular sections thro

In the Fribourg area I
in the Upper Marine M
to the south (Hoffman, 1
represent the major feed
marine seaway. A *coas*
(Allen and Homewood,
and distributary and tid
constructed of thick, elo
intershoal swales. The
coquinas deposited as gia

Wave ripple-marks are
shore facies belts. Homew

$$P = \rho g H^2 C_g / 8 \quad (20)$$

Group velocity can be obtained from Wiegel's (1964) Airy wave transformations as the dimensionless ratio C_g/C_∞ (Fig. 6) by use of the expression for wave phase velocity (celerity):

$$C = L/T = (gT/2\pi) \tanh(2\pi h/L) \quad (21)$$

where $C = C_\infty = gT/2\pi$ in deep water.

Energy flux for reconstructed wave conditions should decrease in shallowing waters, the ratio of deep-water energy flux to shallow-water energy flux providing an index of power attenuation. Homewood and Allen (1981) used estimates of energy flux to provide modern analogues to the Miocene Sea of Switzerland by comparison with the energy flux (wave power) data of Coleman and Wright (1975) and Wright and Coleman (1973).

THE UPPER MARINE MOLASSE OF SWITZERLAND

The wedge of Tertiary clastic sediments north of the Swiss Alps is traditionally subdivided into four units (Matter et al., 1980; and Fig.7A). The lowermost, of Oligocene age, is termed the Lower Marine Molasse and represents offshore mudstones with storm sandstones and culminates in a wave-dominated shoreline sequence. The overlying unit, the Lower Freshwater Molasse comprises predominantly fluviatile clastic sediments with some playa and lacustrine sediments. The third unit is the Upper Marine Molasse of Miocene (Burdigalian) age, consisting of wave- and tide-dominated shallow marine sandstones and the conglomerates of fringing fan-deltas. The uppermost unit, the Upper Freshwater Molasse is composed of alluvial fan and fluviatile clastics and lacustrine deposits.

The Upper Marine Molasse was deposited in a peri-Alpine depression north of the Alps (Fig.7B) which extended eastward to the Austro-Vienna basin and southwestward into France. Although wave-formed structures occur throughout the Upper Marine Molasse, the present study concerns the area in the vicinity of Fribourg where road cuttings and river gorges provide spectacular sections through the marine sand bodies.

In the Fribourg area Homewood (1978, 1981) described four facies belts in the Upper Marine Molasse (Fig.7C). The *proximal facies belt*, restricted to the south (Hoffman, 1960), is composed of thick fan-delta deposits which represent the major feeder systems of sediments from the Alpine hills to the marine seaway. A *coastal facies belt* contains abundant tidal sandwaves (Allen and Homewood, 1984) interbedded with intertidal sandflat deposits and distributary and tidal channel sandstones. The *nearshore facies belt* is constructed of thick, elongate subtidal shoals with shoal crevasse deltas and intershoal swales. The *offshore facies belt* contains sandy and pebbly coquinas deposited as giant-sized flow-transverse tidal bedforms.

Wave ripple-marks are very common in the coastal, nearshore and offshore facies belts. Homewood and Allen (1981, pp.2540—2543) summarized

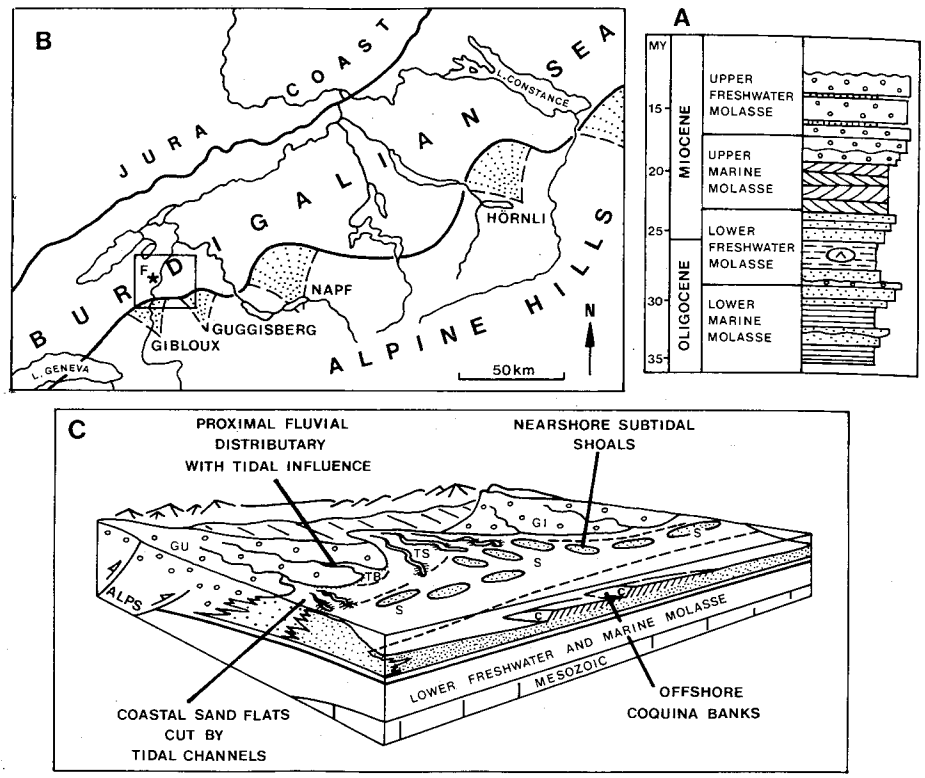

Fig.7. *A*. The four lithostratigraphic subdivisions of the Swiss Molasse after Matter et al. (1980). *B*. Palaeogeographic map of the Upper Marine Molasse of Switzerland with location of major fan-deltas, after Hofmann (1960), Rigassi, in Matter et al. (1980) and Lemcke (1981). *F* marks city of Fribourg. *C*. Diagrammatic reconstruction of distribution of facies belts in the Fribourg area during Burdigalian (Miocene) times (not to scale). *GI* = Gibloux fan; *GU* = Guggisberg fan; *TB* = transverse bars in tidally influenced distributaries; *TS* = tidal sandwaves in coastal belt; *S* = elongate subtidal shoals in nearshore belt; *C* = coquina banks in offshore belt. After Homewood and Allen (1981).

the major findings of a study of ancient wave and tide conditions from these facies belts.

Reconstructed sea conditions

The wave ripple-marks measured in the field possess the symmetries and steepnesses shown in Fig.8. Care was taken to omit ripple-marks which were of questionable origin, in particular those resulting from probable combined flows of waves superimposed on tidal currents. Such ripple-marks were somewhat more asymmetric and were commonly associated with the flanks of tidal sandwaves. A large number of ripple-marks have steepnesses (large VFI) that make estimation of ancient wave conditions hazardous because of the wide range of possible orbital diameters. Fifty-three out of 150 ripple-

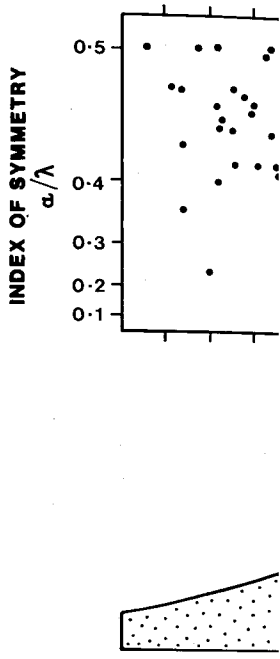

Fig.8. Plot of an index o
wave ripple-marks from t
Allen (1981).

marks are clearly of
dence, and only three
λ_{max} in eq.2 (Fig.9).
and difficulties of acc
the threshold conditi
orbital diameter and o

For each locality a
formative waves over
of *H*, *L* and *h* were t
this way, an impressi
ripple-marks formed
Table I.

Water depths unde
but in extreme cases
cally have been resp
perhaps up to 60 m.
associations. Furtherm
sandwaves showing s
Illens, map co-ord. 5

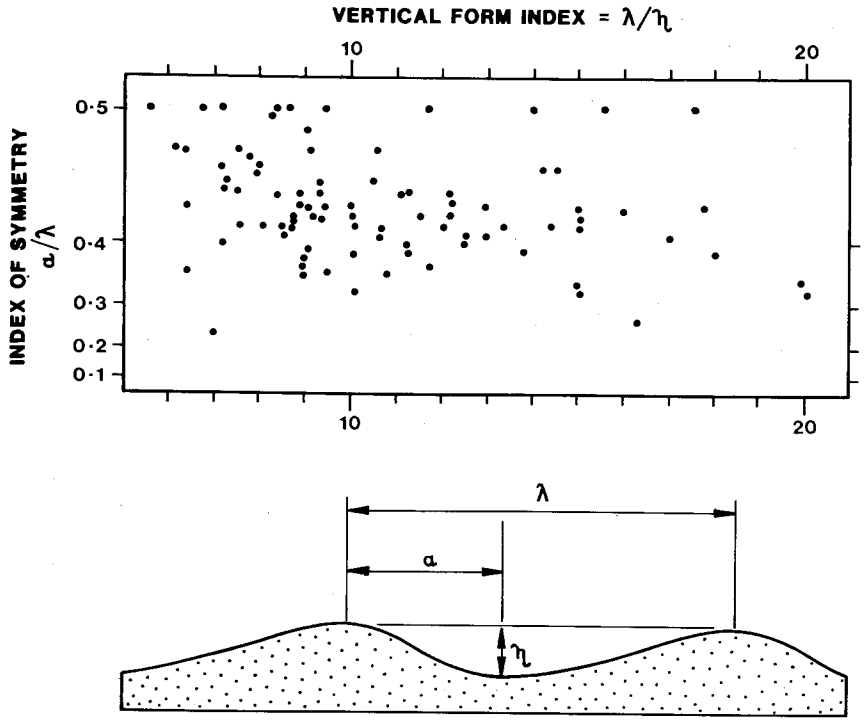

Fig.8. Plot of an index of symmetry against ripple steepness (vertical form index) for wave ripple-marks from the Upper Marine Molasse near Fribourg. After Homewood and Allen (1981).

marks are clearly of the vortex type, where eq. 1 can be used with confidence, and only three of these 53 ripple-marks had a spacing greater than λ_{max} in eq.2 (Fig.9). Bearing in mind the original scatter of data from eq.1 and difficulties of accurate field measurements, it is justifiable to simply use the threshold condition for vortex ripples in estimating wave period from orbital diameter and orbital velocity (Fig.10).

For each locality a table was constructed giving lengths and heights of formative waves over a range of water depths. Unreasonable combinations of H, L and h were then eliminated according to wave breaking criteria. In this way, an impression of the maximum water depths at which the wave ripple-marks formed was obtained. An example for one locality is given in Table I.

Water depths under formative waves were in most cases less than 25 m, but in extreme cases very high waves near the breaking limit may theoretically have been responsible for the wave ripple-marks in deeper waters, perhaps up to 60 m. Such large water depths are unlikely from the facies associations. Furthermore, the association of wave ripple-marks with tidal sandwaves showing shallow-stage run-off patterns and miniripples (as at Illens, map co-ord. 574.50/176.50, Swiss topographic maps No. 252) and

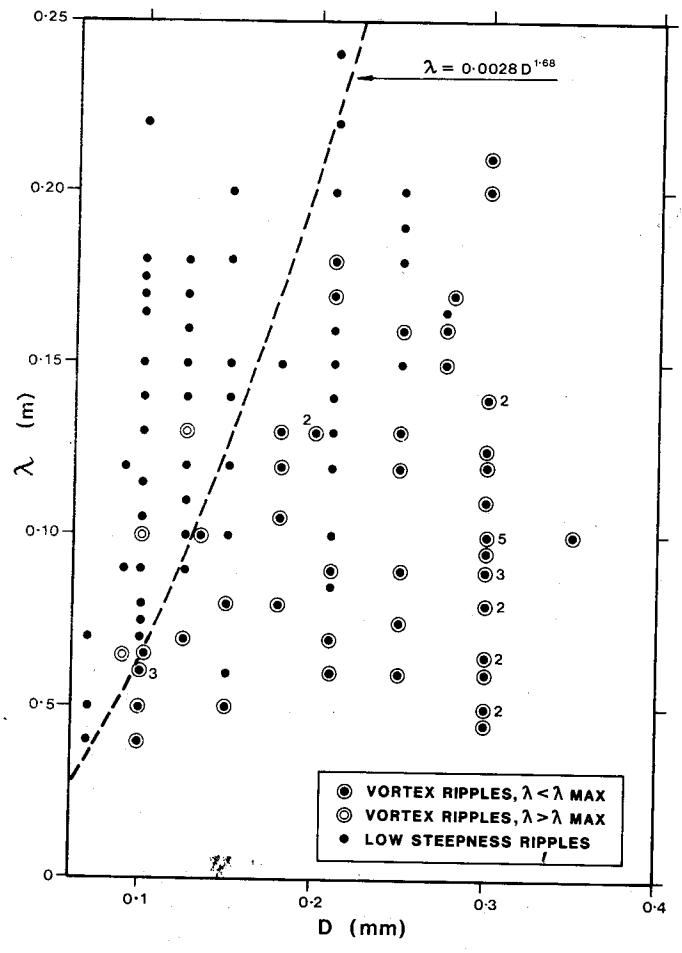

Fig.9. Plot of median grain size against ripple spacing showing the ripple spacing at which the linear relationship between orbital diameter and ripple spacing (eq.1) breaks down (dashed line). Double black circles, vortex ripples, VFI < 7.5; double open circles, vortex ripples with $\lambda > \lambda_{max}$; small dots, low-steepness ripples, VFI > 7.5. Number of superimposed data points also indicated for vortex ripples.

swash bars or flood ramps (as at Fribourg, 578.90/184.70 Map 242) suggests that water depths were shallow, and most wave ripple-marks may have been produced under modest fair-weather waves.

The variability of reconstructed wave conditions between localities is not great, but it may be explained by the relative exposure or sheltering of sub-environments from wave attack and to the viscissitudes of depth during the tidal cycle. In the case of the offshore facies comprising coquina banks, the reconstructed wave periods are generally about 3 s and water depths must have been less than 10 m for formative waves. Since these ripple-marks originate from the facies most distal from the shoreline in the south, it is inconceivable that more proximal facies were deposited in water depths

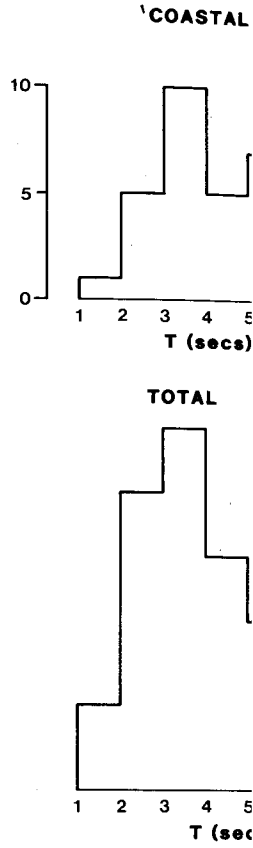

Fig.10. Histograms of
coastal, nearshore and
curve for total. Assum
data only.

TABLE I

Example of work-shee
water depths. Asterisk
in text and caption to F

Water depth (h)	(h/L_∞)	(L/L
0.5	0.019	0.33
1.0	0.038	0.48
5.0	0.192	0.85
10.0	0.385	0.99
20.0	0.769	1.00

Locality: Côtes vers le L
4.08 s. Deep-water wave

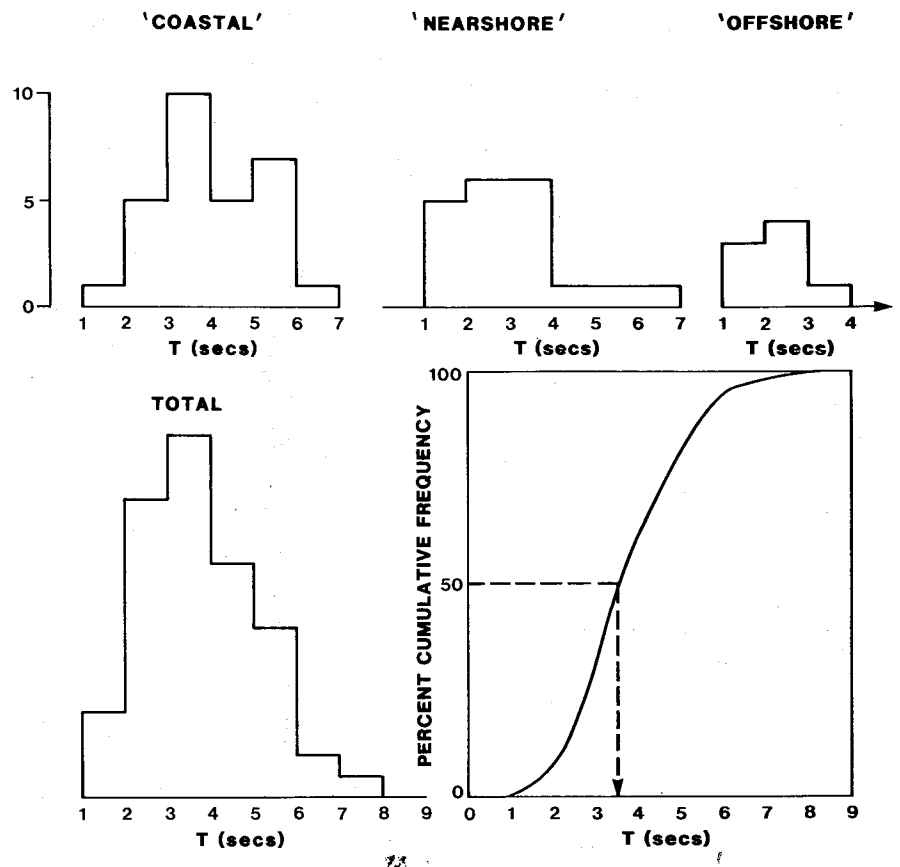

Fig.10. Histograms of calculated maximum wave periods of formative waves for the coastal, nearshore and offshore facies belts and histogram and cumulative frequency curve for total. Assumes the threshold condition and eq.1, utilizing vortex ripple-mark data only.

TABLE I

Example of work-sheet for each locality showing wave transformations in shallowing water depths. Asterisk at h = 20 m indicates unstable wave conditions. Terms defined in text and caption to Fig.6; h, L and H are in metres

Water depth (h)	(h/L_∞)	(L/L_∞)	(H/H_∞)	Shoaling coefficient (n)	(C_g/C_∞)	Surface wavelength (L)	Surface wave height (H)
0.5	0.019	0.33	1.30	0.97	0.33	8.58	0.06
1.0	0.038	0.48	1.10	0.93	0.42	12.48	0.08
5.0	0.192	0.85	0.91	0.68	0.59	22.10	0.31
10.0	0.385	0.99	0.99	0.53	0.53	25.74	0.91
20.0	0.769	1.00	1.00	0.50	0.50	26.00	9.8*

Locality: Côtes vers le Lac, Estavayer — Yverdon Road. Mean of maximum wave periods: 4.08 s. Deep-water wave length: 26.0 m.

substantially greater than this. The apparent landward increase in period of formative waves (Fig.10) may be due to a steadily increasing fetch for the northerly or westerly winds, as the Jura coast became more distant and the Alpine shore was approached.

The calculated values of wave power (or energy flux) fall within a wide range of approximately 10^8—10^6 erg s^{-1}. It must be stressed that calculated wave power values are highly sensitive to estimated water depth since h determines the height of formative waves. Nevertheless, bearing in mind the probable errors, it is possible to compare the wave power at the coast of the Burdigalian Sea in the Fribourg area to that of the Danube, Ebro, Niger and Nile deltas (Table II; Coleman and Wright, 1975). In contrast, the wave-dominated deltas such as the São Francisco and Senegal are moulded by considerably more powerful waves than those estimated for the Burdigalian Sea. Delta morphology is also a function of river input (discharge effectiveness index) and tidal range. Homewood and Allen's (1981) plots using wave power, discharge effectiveness index and tidal range as the three controlling parameters suggested that the closest affinities of the Burdigalian coastal systems in the Fribourg area lie with the present-day deltas of the Niger and possibly Burdekin and Klang.

Comparing the wave power calculated for the offshore coquina bank facies to that of the coastal swash bar or flood ramp facies, representing the passage from the open Burdigalian seaway to the Alpine coast, there appears to have been a wave attenuation of between 50:1 and 100:1.

CONCLUSIONS

Further case-studies of wave-influenced sedimentary sequences are required to broaden the presently inadequate data base. Substantial progress

TABLE II

Year-average wave powers for seven of the world's major deltas and estimated values for the Burdigalian Sea of western Switzerland (Fribourg area). Wright and Coleman's (1973) data have been converted to metric c.g.s. units. The Fribourg molasse values are derived from formative waves in 10 m water depth and in depths of less than 2 m for shoreline wave powers

Delta	Year-average wave power at 10 m contour erg $s^{-1} \times 10^7$	Year-average wave power at shoreline erg $s^{-1} \times 10^7$
Mississippi	190	0.041
Danube	49	0.037
Ebro	172	0.155
Niger	107	2.01
Nile	128	10.17
São Francisco	598	30.37
Senegal	285	114.72
Fribourg Molasse	10—50	0.1—1.0

in the quantification of ancient wave conditions can only be made possible by advances in our knowledge of the relationship between near-bed orbital diameter of water particles and ripple-mark spacing. In this respect, linkage of characteristic ripple geometry or internal structure with flow parameters is necessary.

The reconstructed sea conditions of the Miocene (Burdigalian) Sea in the Fribourg area of western Switzerland are of moderate period waves (3—6 s). Fetch lengths for such waves were of the order of 100 km, placing some constraint on the minimum size of the seaway. The estimated wave power of the Burdigalian Sea indicates an affinity with sea conditions off deltas such as the Ebro and Danube, located in semi-restricted seas, but tidal range was substantially larger than in these two examples.

ACKNOWLEDGEMENTS

I am grateful to John Allen, Peter Homewood and Darwin Spearing for their useful comments on the manuscript. Data were collected with the financial support of the Swiss National Science Foundation, Project 2.242-0.79.

REFERENCES

Allen, G.P., Laurier, D. and Thouvenin, J., 1979. Etude Sédimentologique du Delta du Mahakam. Notes et Mémoires No.15, Compagnie Française des Pétroles, Paris.

Allen, J.R.L., 1979. A model for the interpretation of wave ripple-marks using their wavelength, textural composition and shape. J. Geol. Soc. London, 136: 673—682.

Allen, P.A., 1981a. Wave-generated structures in the Devonian lacustrine sediments of SE Shetland, and ancient wave conditions. Sedimentology, 28: 369—379.

Allen, P.A., 1981b. Some guidelines in reconstructing ancient sea conditions from wave ripple marks. Mar. Geol., 43: M59—M67.

Allen, P.A. and Homewood, P., 1983. Mechanics and evolution of a Miocene tidal sand-wave. Sedimentology, 31: 63—82.

Bagnold, R.A., 1946. Motion of waves in shallow water. Interactions between waves and sand bottoms. Proc. R. Soc. London, Ser. A, 187: 1—15.

Boersma, J.R., 1970. Distinguishing features of wave-ripple cross-stratification and morphology. Ph.D. Thesis, University of Utrecht, Utrecht, 65 pp. (unpubl.).

Brebner, A. and Reidel, P.H., 1973. A new oscillating water tunnel. J. Hydraul. Res., 11: 107—121.

Bretschneider, C.L., 1966. Wave generation by wind, deep and shallow water. In: A.T. Ippen (Editor), Estuary and Coastline Hydrodynamics. McGraw Hill, New York, N.Y., pp.133—196.

Bucher, W.H., 1919. On ripples and related sedimentary surface forms and their palaeo-geographic interpretations. Am. J. Sci., 47: 149—210, 241—269.

Carstens, M.R., Nielson, F.M. and Altinbilek, H.D., 1969. Bedforms generated in the laboratory under an oscillatory flow: analytical and experimental study. U.S. Army Coastal Eng. Res. Centre, Tech. Memo. 28.

Chan, K.W., Baird, M.H.I. and Round, G.F., 1972. Behaviour of beds of dense particles in a horizontally oscillating liquid. Proc. R. Soc. London, Ser. A, 330: 537—559.

Clifton, H.E., 1976. Wave-formed sedimentary structures — a conceptual model. In: R.A. Davies and R.L. Ethington (Editors), Beach and Nearshore Sedimentation. Soc. Econ. Paleontol. Mineral., Spec. Publ., 24: 126—148.

Coleman, J.M. and Wright, L.D., 1975. Modern river deltas: variability of processes and sand bodies. In: M.L. Broussard (Editor), Deltas, Models for Exploration. Houston Geol. Soc., pp.99—149.

Cook, D.O. and Gorsline, D.S., 1972. Field observations of sand transport by shoaling waves. Mar. Geol., 13: 31—56.

Darbyshire, M. and Draper, L., 1963. Forecasting wind-generated sea waves. Engineering (London), 195: 482—484.

Dingler, J.R., 1974. Wave-formed ripples in nearshore sands. Ph.D. Thesis, Univ. of California, San Diego, Calif., 136 pp.

Dingler, J.R., 1979. The threshold of grain motion under oscillatory flow in a laboratory wave channel. J. Sediment. Petrol., 49: 287—294.

Dingler, J.R. and Inman, D.L., 1977. Wave-formed ripples in nearshore sands. Proc. 15th Conf. Coastal Engineering, pp.2109—2126.

Eckart, C., 1952. The propagation of gravity waves from deep to shallow water. U.S. Nat. Bur. Stand. Gravity Waves, Circ., 521: 165—173.

Harms, J.C., 1969. Hydraulic significance of some sand ripples. Geol. Soc. Am. Bull., 80: 363—396.

Hoffman, F., 1960. Materialherkunft, Transport und Sedimentation im Schweizerischen Molassebecken. Jahrb. St. Gallischen Naturwissensch. Ges., 76: 5—28.

Hom-Ma, N., Horikawa, K. and Hajima, R., 1965. A study on suspended sediment due to wave action. Coastal Eng. Jpn., 8: 85—103.

Homewood, P., 1978. Exemples de séquences de faciès dans la molasse fribourgeoise et leur interpretation. Soc. Fribourg Sci. Nat. Bull., 67: 73—82.

Homewood, P., 1981. Faciès et environnements de depôt de la Molasse de Fribourg. Eclogae. Geol. Helv., 74: 29—36.

Homewood, P. and Allen, P.A., 1981. Wave-, tide- and current-controlled sandbodies of Miocene Molasse, western Switzerland. Bull. Am. Assoc. Pet. Geol., 65: 2534- 2545.

Horikawa, K. and Watanabe, A., 1967. A study of sand movement due to wave action. Coastal Eng. Jpn., 10: 39—57.

Inman, D.L., 1957. Wave generated ripples in nearshore sands. U.S. Technol. Memo. Beach Erosion Board, 100, 42 pp.

Inman, D.L. and Bowen, A.J., 1963. Flume experiments on sand transport by waves and currents. Proc. 8th Conf. Coastal Engineering, 1: 137—150.

Ippen, A.T. and Kulin, G., 1955. The shoaling and breaking of the solitary wave. Proc. 5th Conf. Coastal Engineering, pp.27—49.

Kalkanis, G., 1964. Transportation of bed material due to wave action. U.S. Army Corps Engrs, Coastal Eng. Res. Centre, Tech. Memo., 2, 38 pp.

Kaneko, A. and Honji, H., 1979. Initiation of ripple marks under oscillating water. Sedimentology, 26: 101—113.

Kennedy, J.F. and Falcon, M., 1965. Wave generated sediment ripples. M.I.T. Dept. Civ. Eng. Hydro. Lab. Rept. 86, 55 pp.

Komar, P.D., 1974. Oscillatory ripple marks and the evaluation of ancient wave conditions and environments. J. Sediment. Petrol., 44: 169—180.

Komar, P.D., 1976. Beach Processes and Sedimentation. Prentice-Hall, Englewood Cliffs, N.J., 429 pp.

Komar, P.D. and Miller, M.C., 1973. The threshold of sediment movement under oscillatory water waves. J. Sediment. Petrol., 43: 1101—1110.

Komar, P.D. and Miller, M.C., 1976. The initiation of oscillatory ripple marks and the development of plane-bed at high shear stresses under waves. J. Sediment. Petrol., 45: 697—703.

Le Méhauté, B., Divoky, D. and Lin, A., 1969. Shallow water waves: a comparison of theories and experiments. Am. Soc. Civ. Eng., Proc. 11th Conf. Coastal Engineering, pp.86—96.

Lofquist, K.E.B., 1977. A positive displacement oscillatory water tunnel. Coastal Eng. Res. Centre, Misc. Rep., 77-1, 26 pp.

Lofquist, K.E.B., 1978. Sand ripple growth in an oscillatory-flow water tunnel. Tech. Pap. U.S. Coastal Eng. Res. Centre, 78-5, 101 pp.

Madsen, O.S., 1974. Wave climate of the continental margin (its mathematical description). In: D.J. Stanley and D.J.P. Swift (Editors), The New Concepts of Continental Margin Sedimentation — Sediment Transport and its Application to Environmental Management. Short Course Lecture Notes, Am. Geol. Inst., pp.42—108.

Manohar, M., 1955. Mechanics of bottom sediment movement due to wave action. U.S. Army Corps Engrs, Beach Erosion Bd., Tech. Memo., 75, 121 pp.

Matter, A. et al., 1980. Flysch and Molasse of central and western Switzerland. In: R. Trumpy (Editor), Geology of Switzerland, a Guide Book. Exc. 126A, 26th Int. Geol. Congress, Paris, Schweiz. Geol. Komm., pp. 261—293.

McCowan, J., 1894. On the highest wave of permanent type. Philos. Mag., 5: 351—357.

Miche, R., 1944. Undulatory movements of the sea in constant and decreasing depth. Ann. Ponts Chauss, May—June, July—August, 25—78, 131—164, 270—292, 369—406.

Miller, M.C. and Komar, P.D., 1980a. Oscillation sand ripples generated by laboratory apparatus. J. Sediment. Petrol., 50: 173—182.

Miller, M.C. and Komar, P.D., 1980b. A field investigation of the relationship between oscillation ripple spacing and the near-bottom orbital motions. J. Sediment. Petrol., 50: 183—191.

Mogridge, G.R., 1973. Bedforms generated by wave action. DME/NAE Q. Bull., 1973(2), 41 pp.

Mogridge, G.R. and Kamphuis, J.W., 1973. Experiments on bedform generation by wave action. Am. Soc. Civ. Engr., Proc. 13th Conf. Coastal Engineering, pp.1123—1142.

Neumann, G., 1953. On ocean wave spectra and a new way of forecasting wind-generated sea. U.S. Army Corps Eng., Beach Erosion Board, Tech. Mem., 43, 42 pp.

Newton, R.S., 1968. Internal structure of wave-formed ripple marks in the nearshore zone. Sedimentology, 11: 275—292.

Rance, P.J. and Warren, N.F., 1969. The threshold of movement of coarse material in oscillatory flow. Am. Soc. Civ. Eng., Proc. 11th Conf. Coastal Engineering, pp.487—491.

Reineck, H.E., Singh, I.B. and Wunderlich, F., 1971. Einteilung der Rippeln und anderer mariner Sandkorper. Senckenbergiana Marit., 3: 93—101.

Sleath, J.F.A., 1975. A contribution to the study of vortex ripples. J. Hydraul. Res., 13: 315—328.

Sleath, J.F.A., 1976. On rolling grain ripples. J. Hydraul. Res., 14: 69—80.

Sleath, J.F.A. and Ellis, A.C., 1978. Ripple geometry in oscillatory flow. Univ. Cambridge Dept. Engr. Rept. A/Hydraulics/TR2, 15 pp.

Stone, R.O. and Summers, H.J., 1972. Study of subaqueous and subaerial sand ripples. Univ. S. Calif. Dept. Geol. Sci., Final Rept., 72-1.

Sverdrup, H.U. and Munk, W.J., 1946. Empirical and theoretical relations between wind, sea and swell. EOS, Trans. Am. Geophys. Union, 28: 823—927.

Tanner, W.F., 1967. Ripple mark indices and their uses. Sedimentology, 9: 89—104.

Tanner, W.F., 1971. Numerical estimates of ancient waves, water depth and fetch. Sedimentology, 16: 71—88.

Teleki, P.G., 1972. Wave boundary layers and their relation to sediment transport. In: D.J.P. Swift, D.B. Duane and O.H. Pilkey (Editors), Shelf Sediment Transport: Process and Pattern. Dowden, Hutchinson and Ross, Stroudsbourg, Pa., pp.21—60.

Wiegel, R.L., 1964. Oceanographical Engineering. Prentice Hall, Englewood Cliffs, N.J., 532 pp.

Wright, L.D. and Coleman, J.M., 1973. Variations in morphology of major river deltas as functions of ocean wave and river discharge regimes. Bull. Am. Assoc. Pet. Geol., 57: 370—398.

Yalin, S. and Russell, R.D.H., 1962. Similarity in sediment transport due to waves. Proc. 8th Conf. Coastal Engineering, pp.151—171.